Field and current-induced magnetization reversal studied through spatially resolved point-contacts

Magne Saxegaard,[1] DeZheng Yang,[1] Erik Wahlström,[1,a)] Rimantas Bručas,[2] and Maj Hanson[2]

[1]*Institutt for fysikk, NTNU, NO-7491 Trondheim, Norway*
[2]*Institutionen för teknisk fysik, Chalmers tekniska högskola, SE-412 96 Göteborg, Sweden*

We present results from scanning tunneling microscopy based point-contact measurements of the local resistance in octagon shaped, $Co(20 \text{ nm})/Cu(5 \text{ nm})/Fe_{19}Ni_{81}(2.5 \text{ nm})$ spin-valve rings. Through this technique one can detect the magnetoresistance with spatial resolution, and link it to magnetic domain wall motion within the ring. Measurements with varying currents indicate current-induced effects leading to offsets in the magnetic fields required for magnetic switching. The offsets can be attributed to current-induced spin-transfer torque effects for the thin $Fe_{19}Ni_{81}$ layer and to Oersted field effects for the thick Co layer. © *2010 American Institute of Physics.* [doi:10.1063/1.3407539]

I. INTRODUCTION

Magnetic nanostructures and spin-dependent transport are important topics in both current research and development of information technology.[1–4] Special attention has been given to circular and ring shaped magnetic structures (cf., e.g., Refs. 5–14), as they allow both low magnetic stray fields and reproducible magnetic switching, important features in magnetic storage devices.

Transport measurements and sample characterization are often limited to average measurements of multiple structures due to, e.g., macroscopic electrodes or spot sizes of magneto-optical methods. Nanometer sized electrical point-contacts enable local probing of the transport properties of magnetic layered structures.[15–18] By combining point-contact measurements with the imaging mode of a scanning tunneling microscope (STM), the local transport properties of individual laterally shaped structures may be measured.[19] Spatially resolved point-contact measurements allow the study of fundamental physical phenomena such as magnetic domain structures and magnetization reversal processes. In addition, they may provide information about the interplay between magnetization and currents through the spin-transfer torque (STT) effects[20,21] and the Oersted field effect.[22,23]

In this study, we investigate the magnetization state and reversal paths of $Co/Cu/Fe_{19}Ni_{81}$ octagon shaped spin-valve rings with STM based point-contacts in combination with magnetic force microscopy (MFM) and micromagnetic simulations. The giant magnetoresistance (GMR) effect[24,25] is utilized as a contrast mechanism for the magnetization state during point-contact measurements in external magnetic fields. In addition, current-induced effects are investigated by applying different levels of current through the point-contact.

The data from our ~300 successful point-contacts cover large variations in the magnetoresistance response of the spin-valve octagons. In this study, we choose to focus on the common denominators and general trends presented in averaged values and support this by a few illustrative examples. Discussion of deviations and exotic features in the individual curves is thus kept to a minimum in this report.

II. EXPERIMENTAL METHOD

A multilayer film of $Cu(100 \text{ nm})/Co(20 \text{ nm})/Cu(5 \text{ nm})/Fe_{19}Ni_{81}(2.5 \text{ nm})/Cu(20 \text{ nm})$ was prepared on Si/SiO substrates by dc magnetron sputtering, as described earlier.[19] Selective switching between states of parallel (P) and antiparallel (AP) alignment is allowed by the different coercivities of the soft permalloy layer and the hard cobalt layer. Furthermore, the structure offers a minimum of interfaces and a good matching of the electron bands at the Fermi level.[26] The 100 nm Cu layer acts as the bottom electrode in the resistivity measurement. The top Cu layer serves both as capping, preventing oxidation of the ferromagnetic permalloy during patterning, and as a material suitable for point-contact formation while leaving the ferromagnetic layers intact during indentation.

The multilayer film was patterned by e-beam lithography and ion-beam (Ar^+) milling applying methods that yield elements of well-defined shapes.[27,28] During milling the bottom Cu layer was left unbroken. The spin-valve elements were designed as octagonal rings with inner and outer diameters of 1700 and 2200 nm for large rings and 1133 and 1467 nm for small rings. The vortex magnetization state expected to form at zero field in circular elements (disks) features very low stray fields, a key feature in, e.g., memory application. By removing the high-energy vortex core, rings provide even better control of the vortex state and possibly more reproducible magnetic switching.[5,7] In this experiment, corners were added to the rings (making them octagons) in order to create the necessary domain wall pinning sites for imaging with MFM and measuring spin dependent transport properties.

The structure and quality of the patterns were checked by atomic force microscopy and scanning electron microscopy. MFM images were obtained using commercially avail-

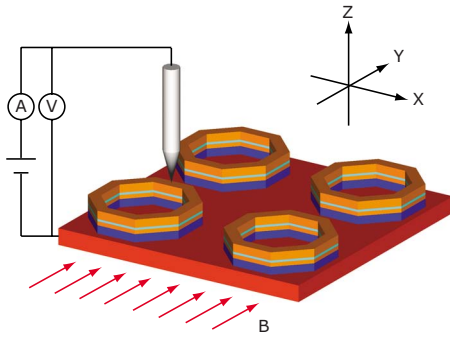a)Electronic mail: erik.wahlstrom@ntnu.no.

FIG. 1. (Color online) Schematic of the experimental setup during point-contact measurements. The STM tip is indented into the top of the sample structure (octagon). GMR curves are measured by simultaneously applying a constant current (A) perpendicular to the sample (z) and a varying in-plane (x,y) magnetic field (B) while recording the voltage drop (V) across the tip and sample.

able high-coercivity cantilevers with CoCr coating. The scan was performed at a lift scan height of 50 nm. The spin-valve elements were checked in the as-prepared state in zero field and thereafter with *in situ* applied magnetic fields B in the range ± 30 mT.

The switching properties of the octagons were also explored by micromagnetic simulations with the OOMMF package and the three-dimensional (3D) OXSII solver.[29] Magnetic saturation moments (M_s), exchange constants (A), anisotropy constants (K_1), and the damping constant (α) were set to standard values of $M_s(\mathrm{Fe_{19}Ni_{81}}) = 8.6 \times 10^5$ A/m, $M_s(\mathrm{Co}) = 14 \times 10^5$ A/m, $A(\mathrm{Fe_{19}Ni_{81}}) = 1.3 \times 10^{-11}$ J/m, $A(\mathrm{Co}) = 3 \times 10^{-11}$ J/m, $K_1(\mathrm{Fe_{19}Ni_{81}}) = 0$, $K_1(\mathrm{Co}) = 520 \times 10^3$ J/m^3 and $\alpha = 0.5$.[29] The copper layer was modeled purely as a spacer layer, with the material constants (M_s, A, K_1) and the exchange interaction between layers set to zero. A compromise between simulation time and an accurate description of the (smaller) sample was achieved by setting the lateral cell sizes to 5 nm and the vertical cell size to 3 nm. Using 256×256 cells in the lateral directions and eight in the vertical direction, the inner and outer diameter of the simulated structure were 990 and 1280 nm and the layer thicknesses $\mathrm{Co}(15\ \mathrm{nm})/\mathrm{Cu}(6\ \mathrm{nm})/\mathrm{Fe_{19}Ni_{81}}(3\ \mathrm{nm})$. This agrees with the standard criterion in micromagnetism that cell sizes should be smaller than the exchange length of the relevant materials,[30] which is approximately 5 nm for both cobalt and permalloy. A selection of simulation steps was repeated with 2.5 nm cell sizes in the x and y direction, but no significant difference was found from the simulation with 5 nm cell sizes. Finally, the simulated magnetic field was run from zero to ± 100 mT in steps of 5 mT.

Imaging and point-contact measurements were performed with an Omicron variable temperature STM in ultrahigh vacuum at temperatures of about 120 K. The STM was fitted with a custom made preamplifier to allow for switching between tunneling current measurements (nA) and point-contact transport measurements (mA).

A schematic representation of the point-contact measurements is given in Fig. 1. Point-contacts were made by indenting the STM tungsten tip 1–8 nm into the top Cu layer of the sample structures. Magnetoresistance curves were measured by simultaneously applying a constant current and a varying

magnetic field while recording the voltage drop across the tip and sample. The current was applied perpendicular to the sample plane (along the z direction), using the STM tip and the bottom sample copper layer as electrodes. The magnetic field was applied in parallel to the sample plane (x direction) using a small electromagnet mounted on the sample holder. In each GMR curve, the magnetic field was applied in a triangular waveform, sweeping from 0 to +80 mT, +80 to −80 mT and −80 to 0 mT at periods of 0.2 s (5 Hz). The root-mean-square value of this waveform (46 mT) was maintained between the point-contacts in order to minimize changes in temperature due to heat dissipated from the electromagnet. The homogeneity of the field was limited by geometry constraints of the electromagnet, varying from about 60 to 80 mT across the 5 mm gap width. The resistance was calculated as the ratio of measured voltage drop and applied current. No lock-in techniques were used.

Current-induced effects were investigated by applying a range of different currents (± 3–± 25 mA) during repeated cycles of the magnetic field sweep. Each point-contact was kept in position for 2 s. This measurement time was limited by computer and data acquisition (DAQ) capacity, as well as the mechanical stability of the contacts. Sweeping the magnetic field at 5 Hz, we were able to record ten GMR curves at different levels of applied current (positive and negative) in each point-contact. In total, data from 332 successful point-contacts on 47 different structures were investigated. In this work, we define the direction of the current as positive for electrons traveling from the cobalt layer to the permalloy layer and the tungsten tip (sample at negative potential, tip at positive potential).

The lateral resolution of the point-contacts are determined by the contact radius and the distribution of current through the sample. Assuming ballistic transport in the contacts, we estimate the contact radius from an average contact resistance of about 15 Ω to be approximately 5 nm.[31] However, we do not expect ballistic transport throughout the entire structure. Classically, the cone angle enclosing 50% of the current flowing in a point-contact through a flat surface into an isotropic medium is roughly 120°,[32] yielding a current cross section radius of about 50 nm at the permalloy and cobalt interfaces. A lateral resolution of 100 nm is expected, and this has been confirmed in a previous study.[19]

III. RESULTS

A. MFM

The magnetic states of the octagonal rings were sampled by MFM. The images presented in Fig. 2 were made after sweeping the magnetic fields to −30 mT (left) and +30 mT (right). The observed magnetization states were found to stabilize at fields of ± 10 mT, corresponding to previously observed switching fields for the permalloy layer in large rings.[19] We thus conclude that the majority of the MFM contrast results from the top permalloy layer.

The final magnetization states observed in Fig. 2 correspond to the so-called onion state. Resembling the cross section of an onion, this state is characterized by two domains aligned along the external field direction with head-to-head
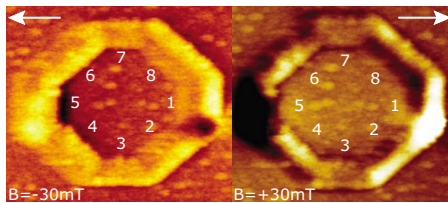
FIG. 2. (Color online) MFM images of a large ring, clearly showing the location of the domain walls. White arrows have been included to show the direction of the external field. Numbers 1–8 are used to label the eight sectors of the ring. Corners are referred to in a clockwise manner, e.g., the corner of sector 1 and 2 is referred to as corner 1.

and tail-to-tail domain walls.[6] The magnetization state for both positive and negative fields are offset from the center-line defined by the direction of the external field. With one domain occupying five of the octagon sectors and the other only three, we denote this asymmetric state the "5/3" onion state in the following discussion.

B. Micromagnetic simulations

The GMR effect depends on the relative orientation of the magnetization in the layers of a spin-valve structure. 3D micromagnetic simulations were performed to clarify the contribution to the GMR effect from the individual layers and to gain a better understanding of how the magnetic states of the layers may affect our measurements.

Starting in a state of random magnetization, the magnetic field is swept in steps of 5 mT from 0 to −100, −100 to 100, and 100 to −100 mT. A selection of magnetization vector plots is shown in Fig. 3. The saturation magnetization states are found to be the onion state with in-plane domain walls for both the permalloy and cobalt layer [Figs. 3(a) and 3(e)]. However, the position of the domain wall in the cobalt and permalloy layer differ, as the larger domain is seen to occupy the *top* five sectors of the cobalt layer ("5/3" onion state) and the *bottom* five sectors of the permalloy layer ("3/5" onion state). In addition, the magnetization at the corners of sectors 1 and 4 of the permalloy layer twists slightly toward the positive field direction.

The reversal from the left-handed onion state to the right-handed onion state of the permalloy layer takes place in several steps. When the field is reduced from −100 to −40 mT, a new set of domain walls is nucleated at the corners of sector 1 and 4. These expand toward each other as the field is further reduced. At −5 mT [Fig. 3(b)] a total of six different domains are seen in the permalloy layer. A gradual transition to a right-handed "5/3" onion state is seen as the field is swept past zero and to +5 mT. Only two narrow domains of left-handed magnetization remain, trapped in the centers of sectors 3 and 7 (not shown). The trapped domain in sector 3 disappears when the field is increased to +45 mT [Fig. 3(c)], while the one in sector 7 remains until the field reaches +85 mT. The positive saturation state of the permalloy layer is found to be a "5/3" onion state, with a slightly reduced total positive magnetization due to twisted magnetization at the corners of sector 5 and 8 [Fig. 3(d)].

The reversal of the cobalt layer takes place in two main steps. First, the bottom half of the ring is reversed at
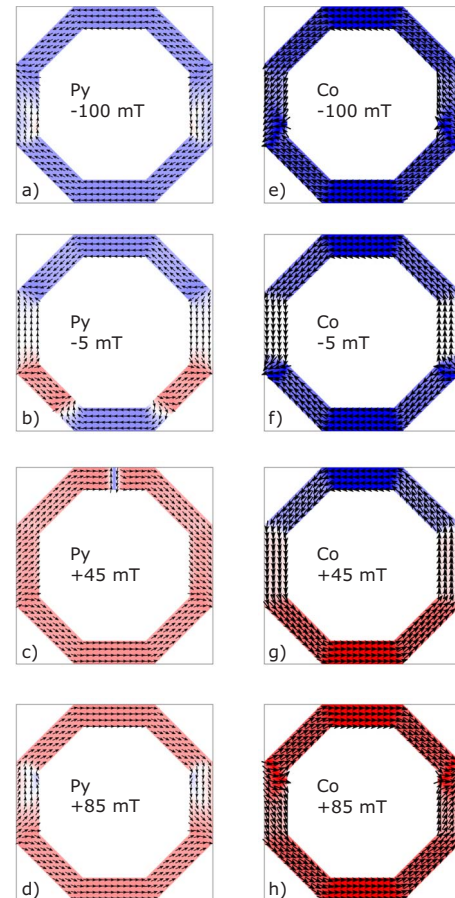

FIG. 3. (Color online) Magnetization vector plots from micromagnetic simulations of the layered structure. Left column (a)–(d) shows the permalloy layer and the right column (e)–(h) shows the cobalt layer. Left and right-handed arrows denote negative and positive magnetization, respectively. The negative external field was applied from right to left and the positive external field from left to right.

+45 mT and the layer enters a flux closure state [Fig. 3(g)]. Second, the top half of the ring is reversed at +85 mT and the cobalt layer enters the positive "3/5" onion state [Fig. 3(h)]. It is interesting to note that the positions of the onion state domain walls are interchanged as the cobalt and permalloy layers are reversed. The reversal process is reproduced in both layers when the field is swept in the opposite direction.

For comparison, individual simulations were run for a single permalloy layer (3 nm) and a single cobalt layer (15 nm). Starting with random magnetization, the field was swept from 0 to 100 mT in steps of 10 mT in the x-direction for both simulations. As expected, due to its negligible anisotropy ($K_1=0$), the permalloy layer was found to enter a symmetric onion state ("4/4") with in-plane domain walls at +10 mT [Fig. 4(a))] and a nearly uniform state with magnetization in parallel with the field as the field was further increased to 50 mT [Fig. 4(b)]. The cobalt layer was found to enter a "5/3" onion state at +90 mT with in-plane domain walls [Fig. 4(d)] via a flux closure state forming at +40 mT [Fig. 4(c)].

Finally, note that the narrow domains observed in sector 3 and 7 in Fig. 3 during the reversal of the permalloy ring are considered to be artifacts of the simulation. These high-
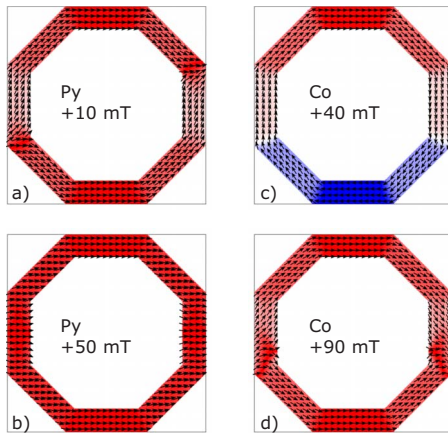
FIG. 4. (Color online) Magnetization vector plots from micromagnetic simulations of single permalloy [(a), (b)] and cobalt [(c), (d)] layers. The positive external field was applied from left to right. The details of these figures are discussed in the text.

energy domains are unphysical and are expected to disappear with the slightest increase in temperature or variation in the direction of the applied field.

C. Point-contact measurements

The example GMR curves shown in Fig. 5 are best discussed by comparison with the simplified case of a spin-valve system with negligible interlayer coupling and only two possible magnetization states (negative and positive saturation) (cf., e.g., Ref. 33). Sweeping the magnetic field from zero to positive saturation, the resistance first changes from low to high as the magnetically soft layer is reversed from a parallel (P) to an antiparallel (AP) alignment with the hard layer (P/AP). Second, the resistance changes from high to low as the magnetically hard layer is reversed and aligned in parallel with the soft layer (AP/P). The exact same transitions will be observed if the external field is swept in the opposite direction. In the following discussion we refer to this as a "normal" GMR curve. We define the critical fields for these P/AP and AP/P transitions as the value of the external field at the *onset* of the change in resistance.
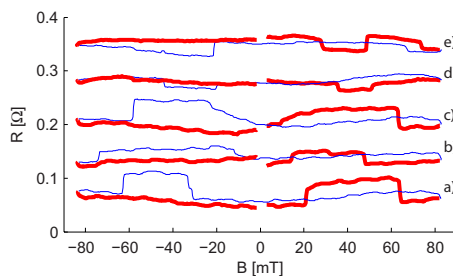

FIG. 5. (Color online) Examples of magnetoresistance curves measured with STM based point-contacts. The curves have been filtered and offset along the R-axis for clarity. (a) Example of a "normal" magnetoresistance curve (from sector 2). (b) Cobalt (AP/P) transitions occurring at very different critical fields, +50 and −70 mT (from sector 7). (c) Small slopes in the permalloy (P/AP) transitions (from sector 3). (d) Inverted curve, with initial and final states of high resistance (from sector 5). (e) Incomplete curve, with different initial and final state (from sector 5). Fat traces are used for positive field sweep and thin traces for negative field sweeps.

TABLE I. Average critical fields with standard deviations in mT for P/AP and AP/P transitions in small (1133/1467 nm) and large (1700/2200 nm) rings. Averages were made from critical fields in all measured magnetoresistance curves.

Size	Co	Py	Py	Co
	AP/P	P/AP	P/AP	AP/P
	$B < 0$	$B < 0$	$B > 0$	$B > 0$
Small	-59 ± 8	-20 ± 11	17 ± 10	54 ± 6
Large	-43 ± 6	-19 ± 11	21 ± 9	40 ± 6

An example of such a "normal" GMR curve measured with STM based point-contacts is shown in Fig. 5(a). The first transition (P/AP) is seen to occur at a critical field of +20 mT, and the second transition (AP/P) at +60 mT. Reversing the direction of the field, the P/AP and AP/P transitions are seen at −30 and −60 mT, respectively. Neglecting the small offset in resistance between positive and negative field sweeps, the initial low resistance state at zero field is recovered at high positive and negative fields (±80 mT).

A few notable variations in the "normal" magnetoresistance curve were observed. One example is given in Fig. 5(b), where the AP/P transitions occur at greatly differing values of the magnetic field, with critical fields of +50 mT and −70 mT in the positive and negative sweep directions. Another example is given in Fig. 5(c), where the slopes of the P/AP transitions are greatly decreased, with the magnetization gradually changing from parallel to antiparallel as the field is increased from zero to ±20 mT.

In addition, "inverted" magnetoresistance curves were observed, as shown by the example in Fig. 5(d). Here, the system is initially in a high-resistance state, featuring "dips" toward lower resistance at critical fields of +35 and −20 mT, and transitions back to high resistance at +50 and −45 mT. An example of incomplete switching is shown in Fig. 5(e). An initial state of high resistance is followed by several transitions to intermediate states and a final state of low resistance, neglecting background offsets in resistance.

Average trends are interpreted with definitions given by the "normal" GMR curve. That is, all transitions are categorized as either P/AP or AP/P, taking place in permalloy or cobalt, respectively. As described, the actual value of the critical fields for these transitions are found to vary in the different types of curves, and some curves are also found to have fewer or more transitions than the four found in a "normal" curve. Nevertheless, some insight may be found by considering average values. Comparing data from small and large rings, the average critical fields for the AP/P transitions are found to be smaller in large rings than small rings, with values of ±40 mT for large rings and ±55 mT for small rings. The permalloy transitions (P/AP) are comparable in both small and large rings, with typical values of ±20 mT, but fairly large standard deviations, see Table I. Note that the average values and standard deviations are calculated from the critical fields in all measured curves, corresponding to hundreds of data points for each average value. This makes the standard deviations in Table I smaller than the standard deviations plotted as error bars in Fig. 7, as these are also
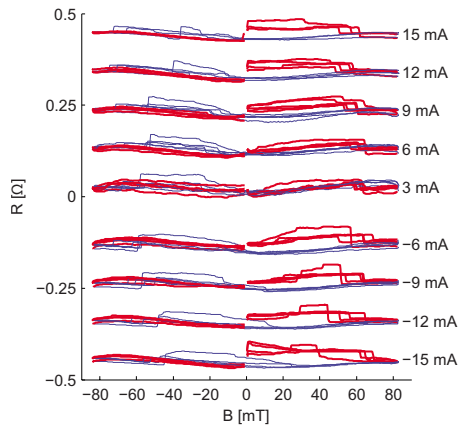
FIG. 6. (Color online) Point-contact magnetoresistance curves as a function of applied sense current, measured in sector 3 of a small ring. (Fat traces used for positive field sweep and thin traces for negative).
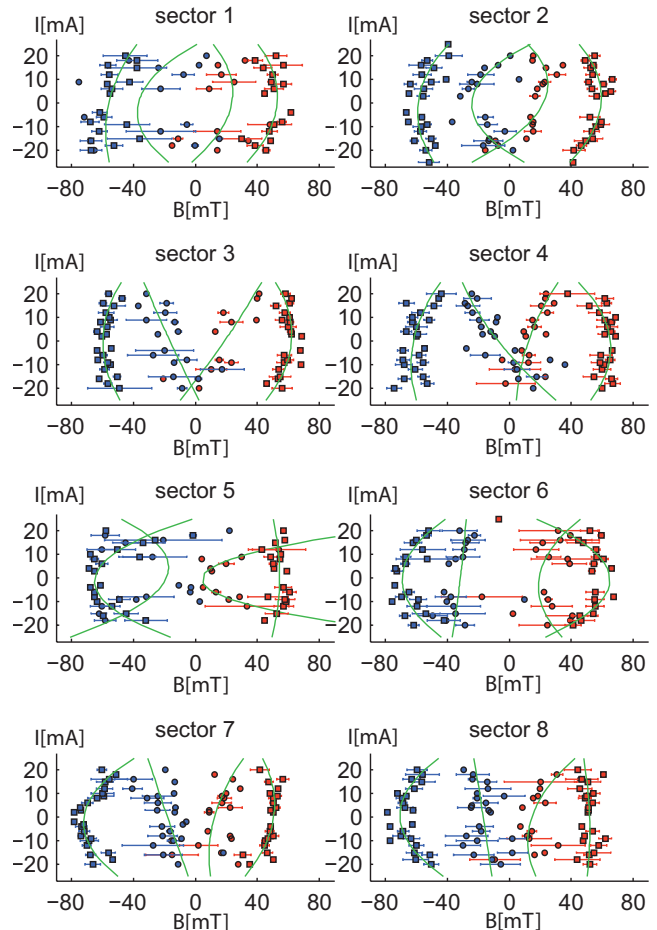

FIG. 7. (Color) Average critical fields with standard deviations as a function of applied sense current in small rings. Critical fields of P/AP transitions are marked with circles and AP/P transitions with squares. Positive field sweeps are shown in red and negative field sweeps in blue. Green lines are second order polynomial fits.

sorted by sector and applied current, reducing the number of data points to tens, rather than hundreds, for each value plotted.

In order to investigate possible current-induced effects, different levels of the sense current were applied through the point-contact during repeated cycles of the magnetic field. Examples of magnetoresistance curves measured at different current levels are shown for a small ring in Fig. 6. The magnetoresistance curves have been shifted along the R-axis according to applied level of sense current. Two features are worth noting. First, the critical field for AP/P transitions is seen to decrease with increasing magnitude of the sense current. Second, the critical fields of the smooth P/AP transitions are seen to increase with increasing current, but in this example, only at negative fields.

These trends are further explored in Fig. 7 by plotting the average value of the critical field as a function of sense current for all transitions in the small rings. A second order polynomial was fitted to the critical fields as a function of applied current in order to visualize possible trends.

For the AP/P transitions, we find a decreasing critical field with increasing magnitude of the sense current in all sectors of the rings. This *symmetric offset* with respect to the direction of the current is fitted reasonably well with the second order polynomial. The current-induced offsets of the P/AP transitions are found to vary with position on the rings. In sectors 3, 4, 7, and 8 we observe a nearly linear shift in the critical field with increasing current. In contrast with the AP/P transitions, the offsets are *antisymmetric* with respect to the direction of the current, featuring small or even negative displacements of the critical field at negative currents and large displacements at positive currents. In sectors 2 and 6, the trends are not so consistent. At negative fields sweeps (blue), we find a tendency for decreasing critical fields with increasing magnitude of the current. At positive fields (blue), the critical field appears to increase with increasing current in sector 2, while the data in sector 6 are too scattered to identify any clear trend. Similarly, in sectors 1 and 5, we find no clear trends, with the exception of the positive field sweep (red) in sector 5, featuring a symmetric increase in critical fields with applied current. In general, the transitions in sec-

tor 1 and 5 are scattered and few due to a limited amount of successful point-contacts and a large variety of magnetoresistance curve types.

IV. DISCUSSION

A. Magnetization states

The onion magnetization state observed with MFM in the top layer of our sample structure agrees well with several studies reported in literature (e.g., Refs. 7 and 10–12). The onion state is also expected as the saturation state for the bottom cobalt layer, due to the domain wall pinning sites introduced by the octagon corners, large outer diameters (1467 and 2200 nm), and narrow widths (300 and 500 nm).[6,8,13] The intermediate flux closure state observed in the cobalt layer of the simulated structure also agrees very well with the above mentioned studies.

The asymmetry of the observed onion states (i.e., "5/3" configuration rather than "4/4"), is explained by the intermediate flux closure state in the cobalt layer, as fewer magnetic moments need to be reversed going to an asymmetric state than a symmetric state [see Figs. 4(c) and 4(d)]. As will be discussed in the following section, the asymmetric onion state in the permalloy layer is explained by stray fields gen-
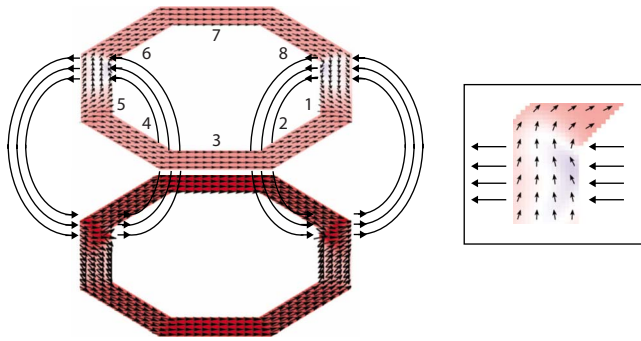
FIG. 8. (Color online) (Left) Sketch of the stray fields generated by the transverse domain walls of the cobalt layer (bottom) acting on the permalloy layer (top) at an external field of +80 mT [cf. Figs. 3(d) and 3(h)]. (Right) Detail of the magnetization in the permalloy layer, as found by micromagnetic simulation. Arrows added to indicate stray fields
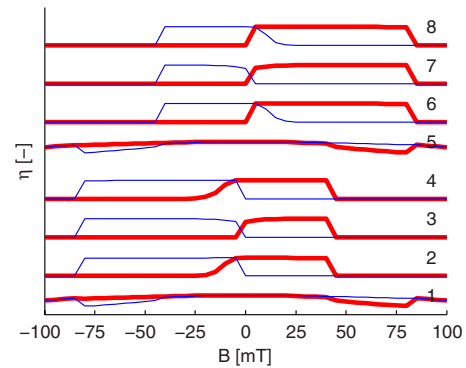

FIG. 9. (Color online) Simplified measure of the GMR effect, η, calculated from the relative orientation of the magnetization vectors in the permalloy and cobalt, as generated by micromagnetic simulation. The eight different curves are average values of η in circular regions from sectors 1–8 of the ring. Fat traces are used for the positive field sweep, thin lines are used for negative field sweep.

erated by onion state domain walls in both layers. From micromagnetic simulations, these domain walls are found to be of a transverse type, with mainly in-plane magnetization. This agrees with observations made by Kläui *et al.*,[9] who found transverse domain walls to dominate over vortex type domain walls in cobalt rings as the width was reduced from 730 to 110 nm and layer thickness from 38 to 2 nm.

A dipolar coupling between the layers is expected due to the stray fields of the transverse domain walls in both layers. An illustration of the cobalt domain wall stray field acting on the permalloy layer is given in Fig. 8. An example is also given in Figs. 3(b) and 3(f), where the stray fields from the cobalt domain walls are seen to nucleate a new pair of domain walls in the permalloy layer, giving rise to a multidomain state as the external field is reduced from saturation. This mechanism has been observed with FMOKE and 3D micromagnetic simulations in similar structures by Hayward *et al.*[11] and Castaño *et al.*[12] In addition, the domain wall stray fields are expected to increase the energy cost of placing the domain walls of the two layers on top of each other. This is demonstrated in Figs. 3(f)–3(h), where the cobalt layer is reversed from a negative "5/3" onion state to a positive "3/5" onion state via a flux closure state. During this reversal, the permalloy layer maintains domain walls in a "5/3" configuration, increasing the energy cost of placing the cobalt domain walls in the same position. The stray fields generated by the transverse domain walls are thus expected to cause interchanging positions of the onion state domain walls in both layers, changing between the "3/5" and "5/3" configuration at each reversal.

The point-contact measurements provide indirect information about the magnetic states of the structures through the GMR effect. In order to compare the information from micromagnetic simulations with these measurements, we consider the relative orientation of the magnetization in the cobalt and permalloy layers as a simple measure of the GMR effect, η. For simplicity, we consider only the scalar product of the magnetization vectors in the two layers and scale this so that the parallel configuration equals zero and the antiparallel configuration equals 1:

$$\eta = \frac{1}{2} - \frac{cos(\theta)}{2}. \qquad (1)$$

Here θ is the angle between the magnetization vectors in the cobalt and permalloy layers. In Fig. 9 we plot average values of η as a function of the external magnetic field from the eight sectors of the ring. Before finding the relative angles, the magnetization is averaged across each layer thickness (Z direction), corresponding to 5 cells $\times$ 3 nm in the cobalt layer and 1 cell $\times$ 3 nm in the permalloy layer. η is further averaged in the lateral directions (X and Y), over an area corresponding to a circle with a radius of 10 cells $\times$ 5 nm, in order to be comparable with lateral resolution of the measured point-contact curves (100 nm).

Three distinct types of simulated GMR curves are observed. The first is found in sector 3 and 7 (oriented in parallel with the applied field) and is characterized by P/AP transitions at ∓ 5 mT and 0 mT as well as AP/P transitions at ± 40 and ∓ 80 mT. The P/AP transitions are explained by the reversal of the permalloy layer from one onion state to the other. The AP/P transition at 40 mT is due to the flux-closure state of the cobalt layer and the AP/P transition at 80 mT is due to the reversed onion state of the cobalt layer.

The second type of curve is observed in sectors 2, 4, 6, and 8 (oblique to the applied field). This is similar to the first, but with a much smaller slope in one of the P/AP transitions. The small slope, approximately 1/20 mT as compared to 1/5 mT in the other transitions, is explained by the multidomain reversal process of the permalloy layer. As the external field is relaxed, the cobalt layer domain wall stray fields increase in relative importance, causing a gradual reversal of the permalloy layer through nucleation of two new walls in the same position as the cobalt layer domain walls.

The third type is observed in sectors 1 and 5, perpendicularly aligned to the applied field. Due to the interchanged positions of the onion state domain walls in the cobalt and permalloy layers, these sectors start and stop with antiparallel magnetization and exhibit "dips" toward parallel alignment at about ± 40 mT. The "dips" in relative orientation are actually never lower than about half the maximum value, and are caused by the transition to the flux-closure state in the cobalt layer. In this intermediate state, the stray fields on the permalloy layer disappear, and the magnetization relaxes to a direction nearly parallel with the external field. Thus, the

relative orientation changes from nearly antiparallel to nearly perpendicular, reducing the calculated value of η. Note that the narrow, trapped domains observed in sector 3 and 7 of the permalloy layer [e.g., in Fig. 3(c)] have not been included in average values of η calculated in Fig. 9, as they are considered artifacts of the simulation, and not representative of the real physics of the sample.

Comparing the simulated GMR curves with the experimental curves in Fig. 5 we find several matches. The characteristic large difference between the critical field of the AP/P transitions at positive and negative sweeps (sectors 3 and 7 of Fig. 9) is reproduced in Fig. 5(b), indicating the intermediate flux-closure state as a possible switching path for the cobalt layer. The small slopes of the simulated P/AP transitions in the oblique sectors are confirmed in Fig. 5(c), but now in both transitions rather than one. The inverted curves of sector 1 and 5 are matched with the example curve in Fig. 5(d), indicating that the positions of the permalloy and cobalt domain walls may be interchanged during reversal.

Several elements of the experimental observations are thus explained by simulation, but there are some discrepancies. The most obvious is the critical fields for the P/AP transitions, with measured average values of ± 20 mT (small and large rings) compared to the simulated transitions occurring basically at zero external field. Possible explanations for this includes a ferromagnetic interlayer exchange coupling due to local stray fields generated by surface roughness (Néel's "orange peel" type[34]), or magnetic anisotropies not accounted for in the simulations. In addition, the two small slope transitions in Fig. 5(c) do not conform with the mechanism of interchanged positions of domain walls, as this would result in only one of the transitions having a small slope, not two. However, it does indicate some form of gradual reversal of a multiple domain state in the permalloy layer.

Finally, the "normal" GMR curve, [Fig. 5(a)] with similar critical fields for both AP/P transitions are not explained by simulations. "Normal" GMR curves demand only two possible magnetization states for both magnetic layers. Our observation may thus be the result of simpler reversal paths, where both the permalloy and the cobalt layer are reversed directly from one onion state to the other.

All elements of the reversal process as described by simulation are thus identified in the measured data, but all features are not present in all data. Key features, such as the onion type saturation state, the intermediate flux-closure state in cobalt and the multidomain reversal process of permalloy are present in the majority of the successful GMR measurements. The strong dipolar coupling and the interchanging position of the cobalt and permalloy domain walls are features that occur more seldom. Possible explanations for this are variations in the relative importance of the domain wall stray field due to inhomogeneities in external field, or structural imperfections. To conclude, our measurements have most likely been made on structures featuring similar magnetization states, with some variations in the observed reversal paths.

B. Current-induced effects

As shown in Fig. 7, the current-induced offsets in the critical field as a function of sense currents exhibit quite strong trends, in spite of a fairly large statistical variation due to contributions from different reversal processes. In the following sections, we argue that the *antisymmetric* offsets seen for the P/AP transitions in some sectors are caused by the (STT) effect,[20,21] while the *symmetric* offsets seen for the AP/P transitions are due to the Oersted field effect. Heating effects are expected to be present as a general background, decreasing the magnetoresistance amplitude with increasing current.[35]

The STT effect can be described as the "inverse" of the GMR effect. For a sufficiently large spin polarized current incident on a ferromagnetic layer, the net transferred spin angular momentum may induce precession or even reversal of the layer magnetization. In a spin-valve geometry, two ferromagnetic layers of different thickness allow the thick layer to act as a "fixed," spin polarizing layer, while the thin layer is "free" to be reversed by the torque transfered from incident spin polarized electrons. The effect, observed by changes in the magnetoresistance of the structure, is inherently *antisymmetric*, as only the magnetization of the "free" layer is allowed to change direction.

In our setup, we expect the sense current applied through the STM tip to exert an effective exchange field on the thin permalloy layer due to spin-polarization and reflection at the thick cobalt layer. Consider, for the sake of simplicity, a nanopillar spin-valve structure with the current flowing essentially in one dimension. The magnitude of this exchange field (H_{STT}) can then be estimated from the STT prefactor (χ) in the dimensionless Landau–Lifshitz–Gilbert equation, as described by Stiles and Miltat:[36]

$$\left(\frac{d\boldsymbol{m}}{d\tau}\right)_{\mathrm{STT}} = -\chi[\boldsymbol{m} \times (\boldsymbol{m} \times \boldsymbol{p})], \qquad (2)$$

$$\chi = \frac{\hbar}{2}\frac{1}{\mu_0 M_s^2}\frac{1}{d}\frac{J}{e}P, \qquad (3)$$

$$H_{\mathrm{STT}} = \chi \cdot M_s. \qquad (4)$$

Here, $\boldsymbol{m}$ corresponds to the magnetization of the free layer, $\boldsymbol{p}$ is a unit vector in the direction of the fixed layer magnetization, and τ corresponds to time. M_s is the saturation magnetization of the free layer, d is the thickness of the free layer, J is the current density through the spin-valve, and P a function describing the spin polarization in the structure. μ_0 is the magnetic permeability of free space, $\hbar$ is the reduced Planck constant, and e is the electron charge.

In our samples, the permalloy layer thickness is 2.5 nm and we assume a magnetic saturation of $M_s(\mathrm{Fe_{19}Ni_{81}}) = 8.6 \times 10^5$ A/m. For simplicity, all spatial variations are neglected, and the polarization function set to a constant value of $P = 0.35$.[37] As mentioned in Sec. II, the current cross section radius is estimated to approximately 50 nm at the cobalt and permalloy interfaces. For a typical sense current of 15 mA, we find a current density of $J \sim 10^8$ A/cm^2. The estimated STT exchange field is then of the order of H_{STT}
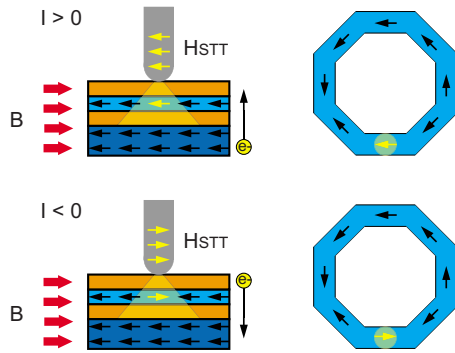
FIG. 10. (Color online) Schematic of the proposed effects of the exchange field H_{STT} on the magnetization of the permalloy layer during field induced reversal. H_{STT} is proposed to interact with a small region below the tip and induces either a parallel or anti-parallel region in the permalloy layer, depending on the direction the current. This is expected to either promote or oppose the reversal induced by the external magnetic field.

$\sim 10^8$ A/m, quite significant compared to the externally applied fields ($\sim 10^3 - 10^4$ A/m). The actual value of the STT exchange field is probably lower, but even reduced by several orders of magnitude, we still expect the STT effect to be observable in our measurements.

The effective exchange field exerted by the spin polarized current is limited to the region probed by the current, but the antisymmetric offsets of the critical fields is a feature of the entire magnetic layer. We propose that the STT exchange field interacts with the permalloy layer in a "nucleation" type model, as illustrated in Fig. 10.

Specifically, the STT field associated with a negative current, H_{STT}^- at the P/AP transitions is expected to nucleate an oppositely aligned domain in the permalloy layer. This will help bring about the field induced reversal and reduce the value of the critical field. The parallel alignment favored by the positive current H_{STT}^+ is expected to have the opposite effect. The externally applied field must overcome the STT exchange field in the active region in order to reverse the permalloy layer, and thus, the value of the critical field is increased. In total, the STT exchange field is expected to cause an antisymmetric offset in the value of the critical field for the P/AP transitions, corresponding well with our observations (cf. Sec. III C and Fig. 7).

The symmetric offsets observed for the AP/P transitions are not explained by the STT exchange field, as we assume it to be negligible for the fixed cobalt layer. (No change in magnetoresistance would be observed if both layers were equally affected by STT). Rather, an explanation is given by the destabilizing effects of the circulating self-magnetic field (Oersted field) of the current applied through the point-contact, $H_{Oe} = I/(2\pi r)$ (cf., e.g., Refs. 22 and 23). Taking $I = 15$ mA and $r = 50$, we find $H_{Oe} \sim 5 \times 10^4$ A/m, i.e., comparable to the applied field, but several orders of magnitude smaller than the STT exchange field. We expect the Oersted field to nucleate vortex like states in the active region below the point-contact, reducing the required external field for reversal of the magnetization in the cobalt layer. The effect is independent of the direction of the applied current and provides symmetric offsets in the critical fields for the AP/P transitions, as observed.

The variations in the current-induced effects with position on the rings are closely related to the magnetization states of the rings. The STT effect scales with the angle between the magnetization in the magnetic layers[20] and we thus expect the antisymmetric offsets to be most clearly visible in regions of uniform magnetization. This corresponds well with our observations, as the antisymmetric offsets are found to be most dominant in sectors 3 and 7, aligned in parallel with the applied magnetic field. The antisymmetric trends observed in sector 4 and 8 further indicate that these oblique sectors may in fact also contain a largely uniform magnetization. In contrast, the perpendicular sectors 1 and 5, expected to contain onion state domain walls, as well as the oblique sectors 2 and 6 do not exhibit antisymmetric trends. This may be interpreted as indirect evidence of nonuniform magnetization, indicating the location of domain walls. Further, the presence of domain walls in both sectors 1, 5, and 2, 6 implies a "4/4" onion state, as well as the previously mentioned "5/3" onion state. In conclusion, we are again most likely observing the effects of several magnetization states and reversal paths of the rings, but with a strong presence of the asymmetric onion state in both the permalloy and cobalt layers.

Finally, note that we do not expect the same lateral variation in the Oersted field induced symmetric offsets of the AP/P transitions. The Oersted field effect is applied as an external field, and is not expected to scale with the magnetization state of the rings.

V. CONCLUSION

The magnetization state and reversal paths of $Co/Cu/Fe_{19}Ni_{81}$ octagons have been determined using a combination of MFM, micromagnetic simulation, and STM based point-contact measurements of the GMR effect. The dominant saturation states were found to be asymmetric ("5/3" and "3/5") onion states for both the permalloy and cobalt layers, but point-contact measurements indicate that a simpler, symmetric ("4/4") onion state may also be present in the some of the octagons. Stray field coupling between the transverse domain walls of the cobalt layer and the permalloy layer were found by simulations and partially confirmed by point-contact measurements.

Different levels of the sense current were found to induce offsets in the critical switching fields for the permalloy (P/AP) and cobalt (AP/P) layers. The antisymmetric offsets observed for increasing currents in the permalloy transitions are explained by an effective exchange field due to the STT effect generated by the applied current. The symmetric decrease in critical field observed for increasing magnitude of the current in the cobalt transitions is explained by the destabilizing effects of the classical Oersted field.

[1]G. A. Prinz, Science **282**, 1660 (1998).
[2]S. A. Wolf, D. D. Awschalom, R. A. Buhrman, J. M. Daughton, S. von

Molnár, M. L. Roukes, A. Y. Chtchelkanova, and D. M. Treger, Science **294**, 1488 (2001).

[3]J. F. Gregg, I. Petej, E. Jouguelet, and C. Dennis, J. Phys. D **35**, R121 (2002).

[4]I. Žutić, J. Fabian, and S. D. Sarma, Rev. Mod. Phys. **76**, 323 (2004).

[5]R. P. Cowburn, D. K. Koltsov, A. O. Adeyeye, and M. E. Welland, Phys. Rev. Lett. **83**, 1042 (1999).

[6]J. Rothman, M. Kläui, L. Lopez-Diaz, C. A. F. Vaz, A. Bleloch, J. A. C. Bland, Z. Cui, and R. Speaks, Phys. Rev. Lett. **86**, 1098 (2001).

[7]O. Kazakova, M. Hanson, A. Blixt, and B. Hjörvarsson, J. Magn. Magn. Mater. **258–259**, 348 (2003).

[8]Y. G. Yoo, M. Kläui, C. A. F. Vaz, L. J. Heyderman, and J. A. C. Bland, Appl. Phys. Lett. **82**, 2470 (2003).

[9]M. Kläui, C. A. F. Vaz, J. A. C. Bland, L. J. Heyderman, F. Nolting, E. Bauer, S. Cherifi, S. Heun, and A. Locatelli, Appl. Phys. Lett. **85**, 5637 (2004).

[10]T. Uhlig and J. Zweck, Phys. Rev. Lett. **93**, 047203 (2004).

[11]T. J. Hayward, J. Llandro, R. B. Balsod, J. A. C. Bland, D. Morecroft, F. J. Castaño, and C. A. Ross, Phys. Rev. B **74**, 134405 (2006).

[12]F. J. Castaño, D. Morecroft, and C. A. Ross, Phys. Rev. B **74**, 224401 (2006).

[13]C. Vaz, M. Kläui, J. Bland, L. Heyderman, C. David, and F. Nolting, Nucl. Instrum. Methods Phys. Res. B **246**, 13 (2006).

[14]C. A. Ross, F. J. Castaño, W. Jung, B. G. Ng, I. A. Colin, and D. Morecroft, J. Phys. D **41**, 113002 (2008).

[15]M. Tsoi, A. Jansen, and J. Bass, J. Appl. Phys. **81**, 5530 (1997).

[16]M. Tsoi, A. Jansen, J. Bass, W. Chiang, M. Seck, V. Tsoi, and P. Wyder, Phys. Rev. Lett. **80**, 4281 (1998).

[17]M. Tsoi, V. Tsoi, J. Bass, A. Jansen, and P. Wyder, Phys. Rev. Lett. **89**, 246803 (2002).

[18]S. J. C. H. Theeuwen, J. Caro, S. Radelaar, L. Canali, L. P. Kouwenhoven, C. H. Marrows, and B. J. Hickey, Appl. Phys. Lett. **77**, 2370 (2000).

[19]E. Wahlström, R. Bručas, and M. Hanson, Appl. Phys. Lett. **88**, 112509 (2006).

[20]J. C. Slonczewski, J. Magn. Magn. Mater. **159**, L1 (1996).

[21]L. Berger, Phys. Rev. B **54**, 9353 (1996).

[22]K. Bussmann, G. A. Prinz, S. F. Cheng, and D. Wang, Appl. Phys. Lett. **75**, 2476 (1999).

[23]J. A. Katine, F. J. Albert, and R. A. Buhrman, Appl. Phys. Lett. **76**, 354 (2000).

[24]M. N. Baibich, J. M. Broto, A. Fert, F. N. V. Dau, F. Petroff, P. Etienne, G. Creuzet, A. Friederich, and J. Chazelas, Phys. Rev. Lett. **61**, 2472 (1988).

[25]G. Binasch, P. Grünberg, F. Saurenbach, and W. Zinn, Phys. Rev. B **39**, 4828 (1989).

[26]D. Y. Petrovykh, K. N. Altmann, H. Höchst, M. Laubscher, S. Maat, G. J. Mankey, and F. J. Himpsel, Appl. Phys. Lett. **73**, 3459 (1998).

[27]M. Hanson, C. Johansson, B. Nilsson, P. Isberg, and R. Wäppling, J. Appl. Phys. **85**, 2793 (1999).

[28]O. Kazakova, M. Hanson, P. Blomqvist, and R. Wäppling, Phys. Rev. B **69**, 094408 (2004).

[29]M. Donahue and D. Porter, National Institute of Standards and Technology Report No. NISTIR 6376, 1999 (unpublished).

[30]W. Rave, K. Ramstock, and A. Hubert, J. Magn. Magn. Mater. **183**, 329 (1998).

[31]Y. V. Sharvin, Zh. Eksp. Teor. Fiz. **48**, 984 (1965) [Sov. Phys. JETP **21**, 655 (1965)].

[32]R. Holm, *Electric Contacts: Theory and Application* (Springer, Berlin, 1967).

[33]T. Shinjo, H. Yamamoto, T. Anno, and T. Okuyama, Appl. Surf. Sci. **60–61**, 798 (1992).

[34]L. Néel, C. R. Acad. Sci. **255**, 1676 (1962).

[35]B. Dieny, P. Humbert, V. S. Speriosu, S. Metin, B. A. Gurney, P. Baumgart, and H. Lefakis, Phys. Rev. B **45**, 806 (1992).

[36]*Spin Dynamics in Confined Magnetic Structures III*, Topics in Applied Physics 101, edited by B. Hillebrands and A. Thiaville (Springer-Verlag, Berlin, Heidelberg, 2006).

[37]L. Bocklage, J. M. Scholtyssek, U. Merkt, and G. Meier, J. Appl. Phys. **101**, 09J512 (2007).